Article

Optimization of Malachite Green Removal from Water by TiO$_2$ Nanoparticles under UV Irradiation

Yongmei Ma [1]**, Maofei Ni** [1,2] **and Siyue Li** [1,]*

[1] Chongqing Institute of Green and Intelligent Technology, Chinese Academy of Sciences, Chongqing 400714, China; mayongmei@cigit.ac.cn (Y.M.); nimaofei000@163.com (M.N.)
[2] University of Chinese Academy of Sciences, Beijing 100049, China
* Correspondence: syli2006@163.com; Tel.: +86-23-6593-5058; Fax: +86-23-6593-5000

check for updates

Abstract: TiO$_2$ nanoparticles with surface porosity were prepared by a simple and efficient method and presented for the removal of malachite green (MG), a representative organic pollutant, from aqueous solution. Photocatalytic degradation experiments were systematically conducted to investigate the influence of TiO$_2$ dosage, pH value, and initial concentrations of MG. The kinetics of the reaction were monitored via UV spectroscopy and the kinetic process can be well predicted by the pseudo first-order model. The rate constants of the reaction kinetics were found to decrease as the initial MG concentration increased; increased via elevated pH value at a certain amount of TiO$_2$ dosage. The maximum efficiency of photocatalytic degradation was obtained when the TiO$_2$ dosage, pH value and initial concentrations of MG were 0.6 g/L, 8 and 10^{-5} mol/L (M), respectively. Results from this study provide a novel optimization and an efficient strategy for water pollutant treatment.

Keywords: TiO$_2$; photocatalytic degradation; malachite green; kinetics process; concentration gradient

1. Introduction

Environmental water pollution is becoming more serious with the development of the social economy and the high density of industrial activity [1,2]. Many countries have suffered water pollution because of the indiscriminate release of untreated wastewater. Among all water, environmental contaminants, synthetic dye, a typical organic pollutant, such as malachite green (MG, $C_{23}H_{25}CN_2$), has been attracting growing attention [3–5]. MG is a common triphenylmethane dye in the textile industry, and it has also been widely used in the fish farming industry as a fungicide, disinfectant, ectoparasiticide, and antibacterial agent [6,7]. However, many researchers have reported that MG and its metabolite leucomalachite green (LMG) are environmentally persistent due to their complex chemical structures. They may also lead to teratogenic, carcinogenic, and mutagenic effects in human beings [8,9]. Thus, MG has been banned or is restricted in many countries. Nevertheless, MG is still illegally used in aquaculture because of its high efficacy and low cost [10]. To minimize the harm caused by MG, it is very important to efficiently remove MG residue from water systems.

In the past few decades, several methods have been applied for MG removal from wastewater. The conventional methods used for MG removal include adsorption, biodegradation, oxidation with ozone or hydrogen peroxide, membrane technology, etc. [11–13]. However, many of these methods are costly, time-consuming, difficult to control, and have high energy consumption and low efficiency. Fortunately, an alternative to the methods mentioned above is advanced oxidation processes, of which photocatalysis is the most popular. The photocatalytic degradation of pollutants through the use of nanomaterials has aroused world-wide attention. In the photocatalysis process, a semiconductor oxide is needed to generate radicals under illuminated light, which are the responsible active species

for removal of hazardous compounds [14]. Among the various photocatalyst, titanium dioxide (TiO$_2$) has been widely used in degrading organic pollutants due to its strong oxidizing power under ultraviolet (UV) light, extraordinary chemical stability, biocompatible features, relatively low cost, and environmental friendliness [15–17]. The principle of TiO$_2$ photocatalytic properties is straightforward: When TiO$_2$ absorbs energy greater than the band gap (approximately 3.2 eV) of itself, electrons can be excited to create electron-hole pairs. These electron-hole pairs migrate to the surface and form hydroxyl groups, which can react with chemicals adsorbed there [18,19]. Therefore, simple, low-cost, and high-efficiency TiO$_2$ used as a photocatalyst to degrade pollutants is considered an attractive and promising treatment for water pollution.

Herein, we report a simple hydrothermal method to prepare TiO$_2$ as an efficient photocatalyst for MG treatment from water under irradiation of UV light. Our procedure for material fabrication is easily operated, has a low cost and is scalable. We tried to determine the optimum operation conditions that can improve the efficiency of MG removal. A series of contrast experiments were performed to confirm TiO$_2$ dosage, pH, and the concentrations of MG, which can maximize the utilization efficiency of TiO$_2$ under UV lights. The whole dynamic process of photocatalytic degradation of MG with TiO$_2$ under UV lights was monitored using a UV-vis spectrophotometer to evaluate the efficiency of MG removal. The results revealed that this simple photocatalytic platform can efficiently remove water pollutants.

2. Results and Discussion

2.1. Characterization of TiO$_2$

TiO$_2$ particles were prepared according to a classical hydrothermal method [19]. Transmission electron microscopy (TEM) and scanning electron microscopy (SEM) images demonstrated that the TiO$_2$ particles were sphere-shaped and had a uniform size distribution, with a diameter around 600 nm (Figure 1 and Figure S1). High resolution transmission electron microscopy (HRTEM) images demonstrated that the lattice fringe, with a spacing of about 0.35 nm, corresponded to the (101) plane of anatase titania. It also revealed that the TiO$_2$ particles were well-dispersed without any aggregation, indicating the stability of these dispersions. The UV-vis spectra showed that TiO$_2$ had an absorbance peak centered at 249 nm (Figure S2).
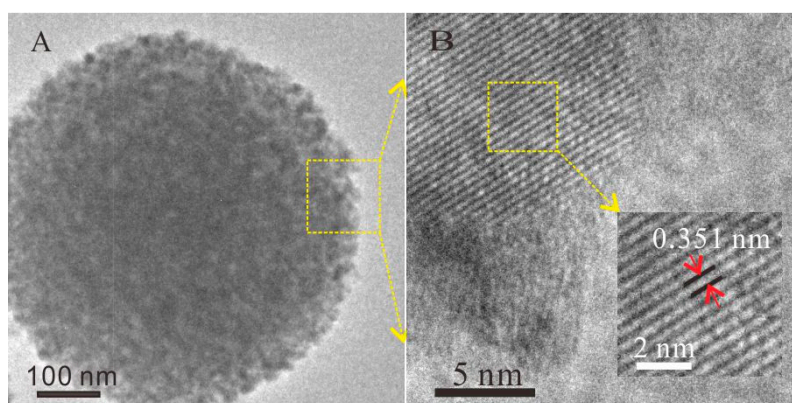

Figure 1. (**A**) TEM image of the TiO$_2$ particle; (**B**) enlarged HRTEM image of details of the TiO$_2$ particle.

The X-ray diffractometer (XRD) pattern of the TiO$_2$ nanoparticles (Figure 2) were in agreement with the standard values of anatase-phase TiO$_2$, with peaks at 2θ = 25.3°, 38.6°, 48.1°, 54.3°, 55.4°, 62.8°, 68.9°, 70.4°, 75.2°, 83.2° (JCPDS files No. 21-1272). Anatase-phase TiO$_2$ has been reported to demonstrate the best photocatalytic degradation activity among various TiO$_2$ crystallinities [20].
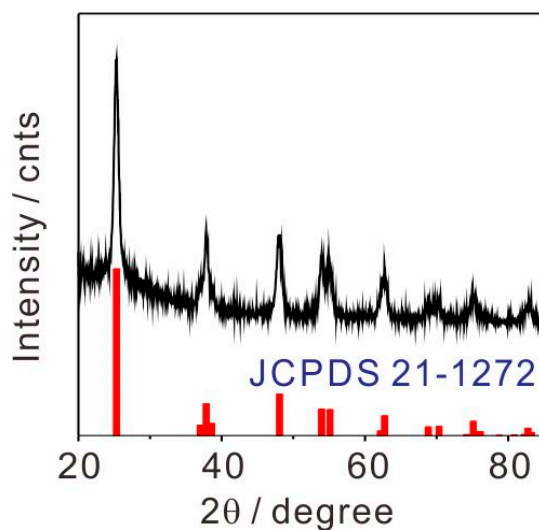
Figure 2. XRD patterns of TiO_2 and the standard XRD patterns of anatase-phase TiO_2 (JCPDS 21-1272).

2.2. Kinetics of Photocatalytic Degradation

2.2.1. TiO_2 Dosage Effect on MG Removal

MG and UV light were used to investigate the photocatalytic activity of TiO_2 particles. TiO_2 particles were dispersed in MG solution (100 mL) in a quartz tube. For obtaining the accurate concentration of MG in photocatalytic degradation, the solution was first stirred for 2 h in the dark to reach an adsorption–desorption equilibrium between the nanoparticles and the solution. Upon UV light irradiation for a designated time, 3 mL of MG aqueous solution was taken out and centrifuged, then the supernatant was used for measuring the absorbance by UV-vis spectroscopy. In practical systems, the optimal operating conditions are very important for the efficiency of pollutant removal [21]. Thus, the optimal amount of TiO_2, pH value and the concentrations of MG would be obtained in the next series of experiments.

Figure 3 demonstrates the influence of amounts of TiO_2 on the efficiency of MG removal. The absorbance spectra of MG (1×10^{-5} M) photocatalyzed by 0.6 g/L TiO_2 particles under UV light irradiation, as a function of irradiation time, are shown in Figure 3A. With the increasing of irradiation time, the absorption intensity of MG at 615 nm gradually decreased, indicating the degradation of MG under the used conditions. The photocatalytic activity of TiO_2 could be evaluated through a comparison between the supernatant concentration at each exposure time to that at time zero. Figure 3B plots time-dependent curves of the C_t/C_0 ratio, an indicator of the degradation degree. C_0 was the original concentration of MG at time zero and C_t was the supernatant concentration of MG after the sample was photocatalyzed by TiO_2 particles under UV light for time t. C_t was obtained from comparing the 615 nm absorbance of the MG supernatant with that of the standard MG solution. After 1 h of irradiation, almost all the MG solution was photocatalytic degraded, regardless of the amount of TiO_2. However, the degradation rates of the different amounts of TiO_2 were different during the whole photocatalytic degradation process. In order to further evaluate the degradation rates mentioned above, Figure 3C shows the kinetics of the photocatalytic degradation reactions, which can be described as a pseudo first-order by Equation (1) [22].

$$\ln \frac{C_t}{C_0} = -kt \tag{1}$$

The rate constants (k, min^{-1}) were calculated from plots of ln (C_t/C_0) vs. irradiation time. The calculated rate constants with 0.4, 0.6 and 0.8 g/L of TiO_2 are 0.0716, 0.0805, and 0.0711 min^{-1},

respectively (Figure 3D and Table 1). The results indicated that the rate constant reached best when TiO_2 dosage was 0.6 g/L under current conditions. The reaction rate constant was found to decrease with increasing TiO_2 dosage up to 0.8 g/L. The probable reason is that light scattering induced by the increased turbidity can reduce the UV light penetration into the bulk suspension and counteract the effect of photocatalyst surface area, resulting in decreased efficiency of MG removal [23,24]. The R^2 of pseudo first-order kinetic model for the photocatalytic degradation of MG with 0.4, 0.6 and 0.8 g/L of TiO_2 are 0.964, 0.995, and 0.976, respectively (Table 1). The R^2 values indicated that there was a better correlation to photocatalytic degradation of MG under TiO_2 particles based on the pseudo first-order kinetic model [25].
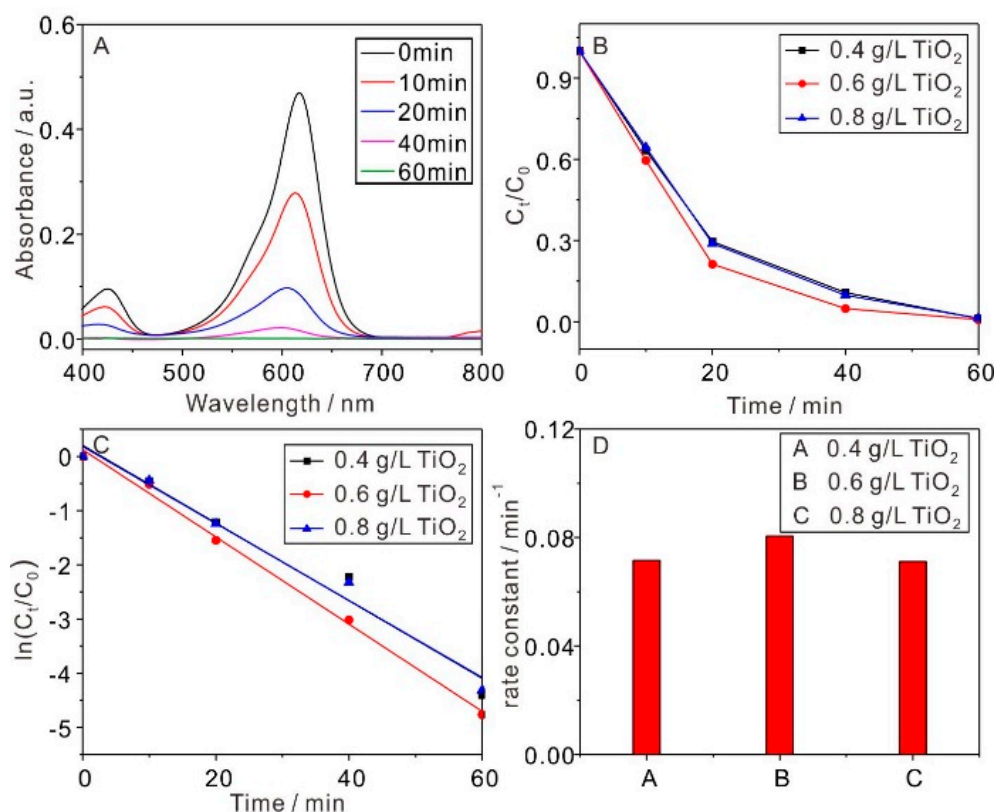

Figure 3. (**A**) Time-course UV-Vis absorbance spectra of MG (10^{-5} M) photocatalyzed by 0.6 g/L TiO_2 under UV light; (**B–D**) The calculated time-dependent ratios of C_t/C_0, first-order degradation rates, and reaction rate constants under UV light with different TiO_2 dosage.

Table 1. Comparison of pseudo first-order model parameters, rate constants (k, min^{-1}) and R^2 under different TiO_2 dosages.

TiO_2 Dosage (g/L)	k (min^{-1})	R^2
0.4	0.0716	0.964
0.6	0.0805	0.995
0.8	0.0711	0.976

2.2.2. Initial Concentrations of MG Effect on the Efficiency of Photocatalytic Degradation

To obtain the capacity of the photocatalyst, different concentrations of MG solution were photocatalyzed using 0.6 g/L TiO_2 under UV light (Figure 4). Figure 4A shows the absorbance spectra of MG (1×10^{-5} M) photocatalyzed using 0.6 g/L TiO_2 particles under UV light irradiation as a function of the irradiation time. Similarly, Figure 4B plots time-dependent curves of the C_t/C_0

ratio to indicate the photocatalytic activity of TiO_2. After 1 h irradiation, almost all MG solution with concentrations of 10^{-5} and 5×10^{-6} M had been photocatalytically degraded. Fifty-six percent of the MG solution (5×10^{-5} M) was degraded, and 64% of MG solution (2.5×10^{-5} M) was degraded after 1 h. Meanwhile, both of the degradation ratios of MG increased continuously with growing irradiation time and reached about 99% after 2 h of irradiation.
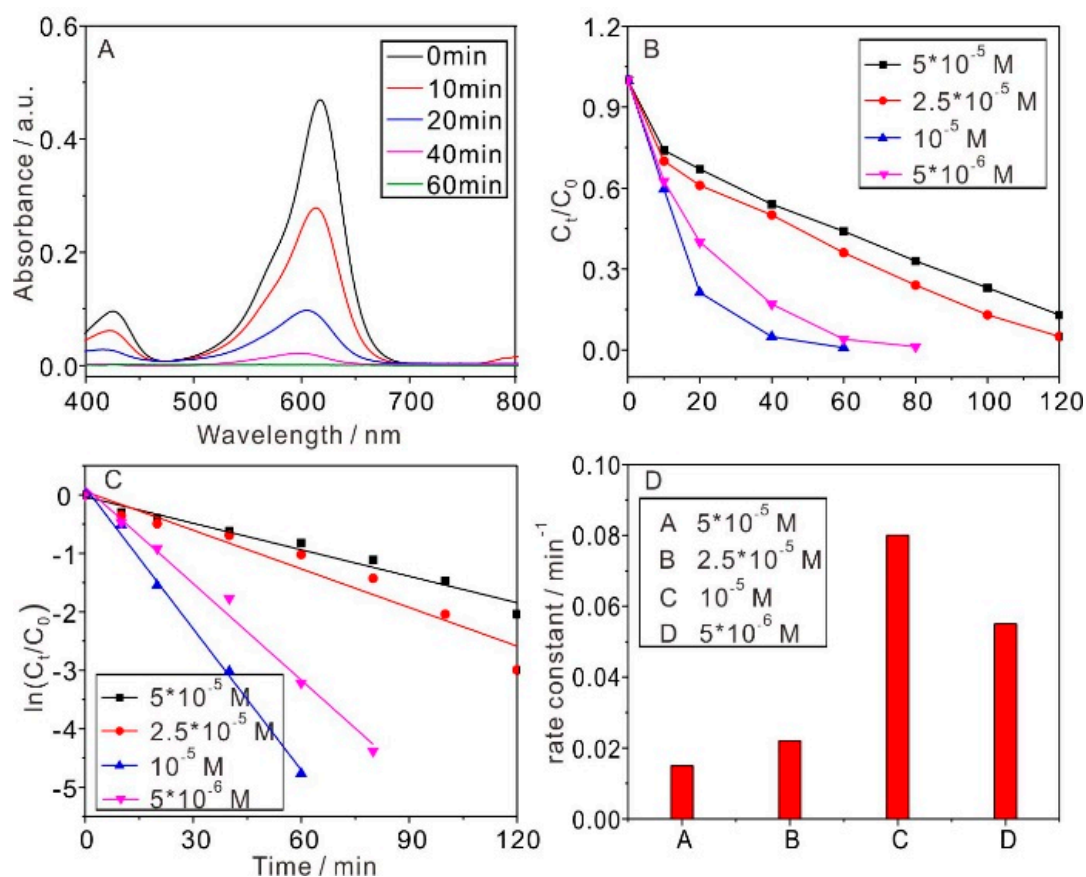

Figure 4. (**A**) Time-course UV-vis absorbance spectra of MG (10^{-5} M) photocatalyzed by 0.6 g/L TiO_2 under UV light; (**B–D**) The calculated time-dependent ratios of C_t/C_0, first-order degradation rates, and reaction rate constants for different concentration of MG photocatalyzed by 0.6 g/L TiO_2 under UV light.

The kinetics of the photocatalytic degradation reactions also can be described as pseudo first-order according to Equation (1) (Figure 4C). The calculated rate constants with the MG concentrations of 5×10^{-5}, 2.5×10^{-5}, 10^{-5} and 5×10^{-6} M were 0.0151, 0.0220, 0.0805 and 0.0550 min^{-1}, respectively (Figure 4D and Table 2), using the methods mentioned above. The results demonstrated that the rate constant reached its best performance when the concentration of MG was 10^{-5} M under the used conditions. Generally, the reaction rate constant will increase by decreasing the concentration of pollutants. However, the ability of the photocatalyst may not show efficiently when the concentration of pollutants is too low. Thus, 10^{-5} M of MG was chosen in subsequent experiments. The R^2 of the pseudo first-order kinetic model for the photocatalytic degradation of MG, with concentrations of 5×10^{-5}, 2.5×10^{-5}, 10^{-5} and 5×10^{-6} M, were 0.965, 0.935, 0.995 and 0.989, respectively (Table 2). The results indicated that the correlation to photocatalytic degradation of MG under TiO_2 particles based on the pseudo first-order kinetic model was good.

Table 2. Comparison of pseudo first-order model parameters, rate constants (k, min^{-1}) and R^2 under different concentrations of MG.

Concentration of MG (M)	k (min^{-1})	R^2
5×10^{-5}	0.0151	0.965
2.5×10^{-5}	0.022	0.935
10^{-5}	0.0805	0.995
5×10^{-6}	0.055	0.989

2.2.3. Effect of pH Values

The pH of the aqueous solution is a significant parameter which influences the efficiency of the photocatalytic degradation at the solution-photocatalyst interfaces [26]. Figure 5 indicates the influence of pH on the efficiency of photocatalytic degradation. The absorbance spectra of MG (1×10^{-5} M) photocatalyzed by 0.6 g/L TiO$_2$ particles at pH = 8 under UV light irradiation, as a function of the irradiation time, are shown in Figure 5A. The time-dependent curves of the C_t/C_0 ratio were also used to indicate the photocatalytic activity of TiO$_2$ (Figure 5B). After 1 h of irradiation, 48%, 90% and 95% of MG solution were degraded at pH = 4, 6 and 8, respectively. When the pH value was 10, the degradation ratio of MG reached about 92% after only 20 min of irradiation.
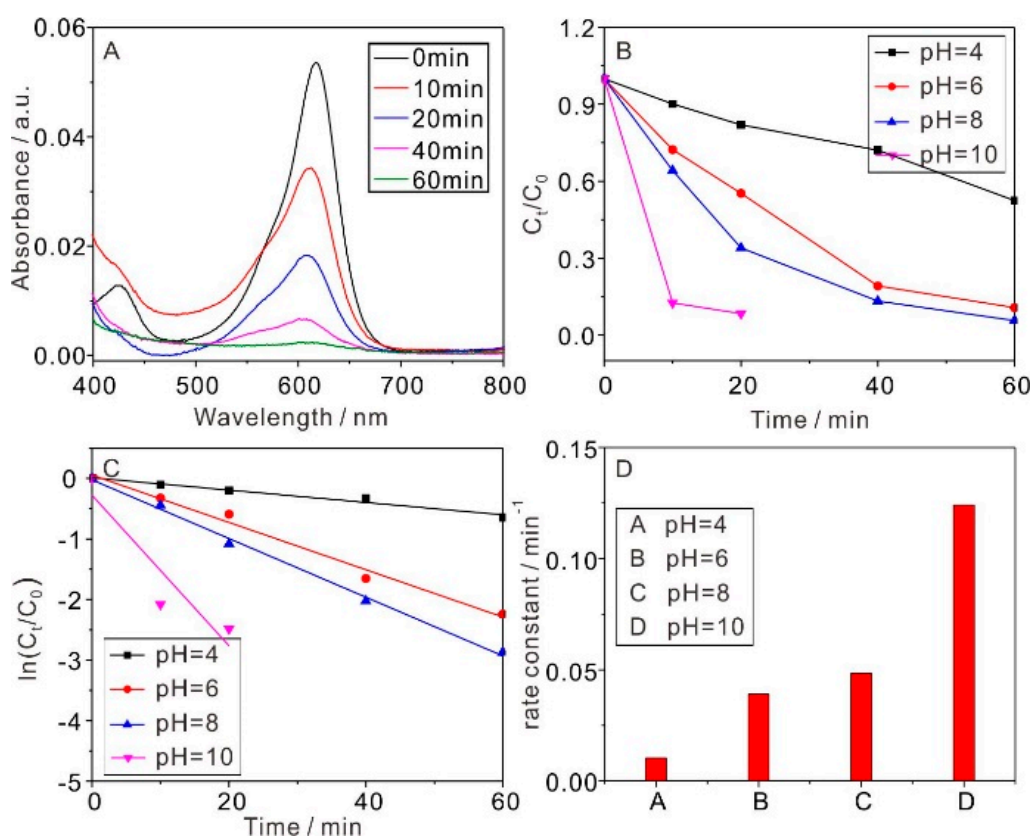

Figure 5. (**A**) Time-course UV-Vis absorbance spectra of MG (10^{-5} M) photocatalyzed by 0.6 g/L TiO$_2$ under UV light at pH = 8. (**B–D**) The calculated time-dependent ratios of C_t/C_0, first-order degradation rates and reaction rate constants for MG (10^{-5} M) photocatalyzed by 0.6 g/L TiO$_2$ with different pH values.

The kinetics of photocatalytic degradation was determined using Equation (1), and the reaction rate constant could be readily derived from the linearly-fitted slope (Figure 5C). The calculated rate

constants at pH = 4, 6, 8 and 10 were 0.010, 0.039, 0.048 and 0.124 min^{-1}, respectively (Figure 5D and Table 3). The results indicated that the reaction rate constant increased with the increasing of the pH values. The surface of the photocatalyst acquired a positive charge when the pH of the solution was less than 7. The amount of MG on the surface of the photocatalyst decreases because of the electrostatic repulsion between the positive surface of photocatalyst and the positive surface of MG. Meanwhile, a photocatalytic degradation reaction generally occurs on the surface of a photocatalyst [27,28]. Thus, acidic conditions were a disadvantage for the reaction. On the contrary, alkaline conditions can promote MG molecules to the surface of the photocatalyst because of the electrostatic attractions between the negative surface of the photocatalyst and the positive surface of MG, resulting in a high efficiency of reaction. The R^2 of pseudo first-order kinetic models for the photocatalytic degradation of MG at pH = 4, 6, 8 and 10 were 0.961, 0.983, 0.995 and 0.737, respectively (Table 3). The results indicated that the correlation to the photocatalytic degradation of MG under TiO_2 particles based on the pseudo first-order kinetic model was good, except for when the pH value was 10. In general, water is weak to mildly alkaline in nature, pH = 8 is close to the pH of natural riverine water. Thus, this condition has great practical application potential in photocatalytic treatment. More importantly, the efficiency of reaction at pH = 8 was also good. Overall, the relatively moderate conditions of pH = 8 were better for this reaction.

Table 3. Comparison of pseudo first-order model parameters, rate constants (k, min^{-1}) and R^2 under different pH values.

pH Values	k (min^{-1})	R^2
4	0.01	0.961
6	0.039	0.983
8	0.048	0.995
10	0.124	0.737

2.3. Mechanism of Photocatalytic Degradation

In order to understand the possible mechanisms for the UV-activated photocatalytic degradation activity of TiO_2 nanoparticles, electron spin resonance (ESR) measurements were conducted. The spectra displaying signals with the characteristic intensity 1:2:2:1 for DMPO-·OH adducts was obtained, which indicated that the ·OH radical was formed under the used conditions (Figure S3) [29]. The possible mechanism for the photocatalytic degradation reaction was discussed (Scheme 1). Under the irradiation of UV light, TiO_2 absorption the energy larger than its band gap (approximately 3.2 eV), electrons were excited from the valence band (CB) to the conduction band (VB), creating electron-hole pairs [30]. And then these electron−hole pairs will migrate to the surface and take part in surface reactions. When the excited electrons arrived at the surface, they reacted with the oxygen to form superoxide ·O^{2-} radical anions. The superoxide ·O^{2-} radical anions reacted with H^+, and finally formed hydroxyl radicals (·OH). Meanwhile, holes also reacted with H_2O and formed ·OH [15,31]. Therefore, the organic molecules present in the solution could react with these oxidizing agents to induce oxidative degradation. In addition, the strong oxidizing power of ·OH could oxidize most of the organics to carbon dioxide (CO_2) and water (H_2O).
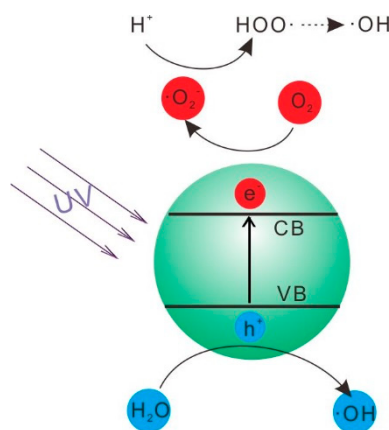
Scheme 1. Illustrated mechanism of UV-activated photocatalysis on TiO$_2$.

3. Materials and Methods

3.1. Chemicals and Materials

Titanium n-butoxide (Ti(OBu)$_4$), alcohol and Malachite green (MG) were obtained from Shanghai Reagent Co. (Shanghai, China), and these chemicals were analytical reagents and were used without further purification. The solutions were prepared with distilled water without further pH regulation, and all experiments were carried out under room temperature (25 °C) in a water system.

3.2. Preparation of TiO$_2$

Titanium *n*-butoxide (Ti(OBu)$_4$) was employed as the Ti source because the hydrolysis rate of Ti(OBu)$_4$ was ca. 150 times slower than that of tetraethyl titanate, Ti(OEt)$_4$ [32]. A typical procedure for preparing titania [33] is described as follows: 300 μL of Ti(OBu)$_4$ was added into 10 mL of ethanol solution. Then, this newly-formed complex precursor solution was transferred into a 60-mL autoclave containing 5 mL of ultrapure water and was heated at 180 °C for 20 h. The resulting product was collected by centrifugation, washed several times with distilled water and ethanol, respectively, and then dried at 60 °C in a drying oven.

3.3. Photocatalytic Experiments

The photocatalytic activities of the TiO$_2$ were evaluated by the degradation of MG under the irradiation of a UV lamp (set at 175 W). In a typical process, the TiO$_2$ particles were dispersed into an MG solution in a quartz tube under different conditions, including the amount of TiO$_2$, pH value and the concentrations of MG. The desired pH of the MG solution was adjusted with 1 M HCl/NaOH to determine the real concentration of MG in the photocatalytic degradation. The solution was then stirred for 2 h in the dark to reach an adsorption–desorption equilibrium between the nanoparticles and the solution. Subsequently, the quartz tube was exposed to irradiation from a UV lamp; 3 mL of MG aqueous solution was intermittently collected at given time intervals for centrifugation, the filtrates measured the absorbance by UV-vis spectroscopy.

3.4. Apparatus

The scanning electron microscopy (SEM) images were taken by a Sirion 200 field-emission scanning electron microscope (ThermoFisher, Waltham, MA, USA). X-ray scattering patterns were determined by analyzing the powder samples on a Philips X-Pert Pro X-ray diffractometer (XRD) (Philips, Amsterdam, Holland) with Cu Ka radiation. Transmission electron microscopy (TEM) images were recorded using a JEOL 2010 high resolution transmission electron microscope (Japan Electronics

Co., Ltd., Tokyo, Japan), operated at an acceleration voltage of 200 kV. The absorbance of the MG solution was measured using a Lambda 35 UV-vis spectrometer (Perkinelmer, Waltham, MA, USA).

4. Conclusions

In summary, TiO_2 nanoparticles were prepared using a simple and efficient method, which has been proved to be a highly-efficient photocatalyst to degrade MG, a representative and worldwide pollutant in water systems. The kinetics of reaction were successfully monitored by UV spectroscopy, and the kinetic process can be well predicted by the pseudo first-order model. The optimal conditions of the key factors, including TiO_2 dosage, concentration of MG and pH values, were determined by analyzing the kinetics of the photocatalytic reaction. The maximum efficiency of MG removal was obtained with the conditions of TiO_2 dosage, pH value and initial concentrations of MG at 0.6 g/L, 8 and 10^{-5} M, respectively. These results provide an efficient strategy to study the photocatalytic degradation of water pollutants.

References

1. Berger, E.; Haase, P.; Kuemmerlen, M.; Leps, M.; Schafer, R.B.; Sundermann, A. Water quality variables and pollution sources shaping stream macroinvertebrate communities. *Sci. Total Environ.* **2017**, *587*, 1–10. [CrossRef] [PubMed]

2. Moskovchenko, D.V.; Babushkin, A.G.; Ubaidulaev, A.A. Salt pollution of surface water in oil fields of Khanty-Mansi Autonomous Area-Yugra. *Water Resour.* **2017**, *44*, 128–138. [CrossRef]

3. Li, L.; Lin, Z.Z.; Peng, A.H.; Zhong, H.P.; Chen, X.M.; Huang, Z.Y. Biomimetic ELISA detection of malachite green based on magnetic molecularly imprinted polymers. *J. Chromatogr. B* **2016**, *1035*, 25–30. [CrossRef] [PubMed]

4. Stead, S.L.; Ashwin, H.; Johnston, B.; Tarbin, J.A.; Sharman, M.; Kay, J.; Keely, B.J. An RNA-aptamer-based assay for the detection and analysis of malachite green and leucomalachite green residues in fish tissue. *Anal. Chem.* **2010**, *82*, 2652–2660. [CrossRef] [PubMed]

5. Maxwell, E.J.; Tong, W.G. Sensitive detection of malachite green and crystal violet by nonlinear laser wave mixing and capillary electrophoresis. *J. Chromatogr. B* **2016**, *1020*, 29–35. [CrossRef] [PubMed]

6. Plakas, S.M.; ElSaid, K.R.; Stehly, G.R.; Gingerich, W.H.; Allen, J.L. Uptake, tissue distribution, and metabolism of malachite green in the channel catfish (*Ictalurus punctatus*). *Can. J. Fish. Aquat. Sci.* **1996**, *53*, 1427–1433. [CrossRef]

7. Safarik, I.; Safarikova, M. Detection of low concentrations of malachite green and crystal violet in water. *Water Res.* **2002**, *36*, 196–200. [CrossRef]

8. Wu, L.; Lin, Z.Z.; Zhong, H.P.; Peng, A.H.; Chen, X.M.; Huang, Z.Y. Rapid detection of malachite green in fish based on CdTe quantum dots coated with molecularly imprinted silica. *Food Chem.* **2017**, *229*, 847–853. [CrossRef] [PubMed]

9. Song, D.; Yang, R.; Wang, C.W.; Xiao, R.; Long, F. Reusable nanosilver-coated magnetic particles for ultrasensitive SERS-based detection of malachite green in water samples. *Sci. Rep.* **2016**, *6*, 22870. [CrossRef] [PubMed]

10. Sivashanmugan, K.; Liao, J.D.; Liu, B.H.; Yao, C.K.; Luo, S.C. Ag nanoclusters on ZnO nanodome array as hybrid SERS-active substrate for trace detection of malachite green. *Sens. Actuators B Chem.* **2015**, *207*, 430–436. [CrossRef]

11. Hashemzadeh, F.; Rahimi, R.; Ghaffarinejad, A. Mesoporous nanostructures of Nb_2O_5 obtained by an EISA route for the treatment of malachite green dye-contaminated aqueous solution under UV and visible light irradiation. *Ceram. Int.* **2014**, *40*, 9817–9829. [CrossRef]

12. Yin, Y.Y.; Li, C.; Song, C.W.; Tao, P.; Sun, M.H.; Pan, Z.L.; Wang, T.H.; Shao, M.H. The design of coal-based carbon membrane coupled with the electric field and its application on the treatment of malachite green (MG) aqueous solution. *Colloids Surf. A Physicochem. Eng. Asp.* **2016**, *506*, 629–636. [CrossRef]

13. Li, X.L.; Zhang, Y.; Jing, L.Y.; He, X.H. Novel N-doped CNTs stabilized Cu_2O nanoparticles as adsorbent for enhancing removal of Malachite Green and tetrabromobisphenol A. *Chem. Eng. J.* **2016**, *292*, 326–339. [CrossRef]

14. Wang, Q.; Chen, C.C.; Zhao, D.; Ma, W.H.; Zhao, J.C. Change of adsorption modes of dyes on fluorinated TiO_2 and its effect on photocatalytic degradation of dyes under visible irradiation. *Langmuir* **2008**, *24*, 7338–7345. [CrossRef] [PubMed]

15. Furukawa, S.; Shishido, T.; Teramura, K.; Tanaka, T. Photocatalytic oxidation of alcohols over TiO_2 covered with Nb_2O_5. *ACS Catal.* **2012**, *2*, 175–179. [CrossRef]

16. Grabowska, E.; Diak, M.; Marchelek, M.; Zaleska, A. Decahedral TiO_2 with exposed facets: Synthesis, properties, photoactivity and applications. *Appl. Catal. B Environ.* **2014**, *156*, 213–235. [CrossRef]

17. Mansouri, F.; Kalankesh, R.L.; Hasankhani, H. The comparison of photo catalytic degradation of dissolved organic carbon (DOC) from water by UV/TiO_2 in the presence and absence of iron ion. *Glob. NEST J.* **2016**, *18*, 392–401.

18. Asuha, S.; Zhou, X.G.; Zhao, S. Adsorption of methyl orange and Cr(Vi) on mesoporous TiO_2 prepared by hydrothermal method. *J. Hazard. Mater.* **2010**, *181*, 204–210. [CrossRef] [PubMed]

19. Qin, S.H.; Cai, W.Y.; Tang, X.H.; Yang, L.B. Sensitively monitoring photodegradation process of organic dye molecules by surface-enhanced Raman spectroscopy based on $Fe_3O_4@SiO_2@TiO_2@Ag$ particle. *Analyst* **2014**, *139*, 5509–5515. [CrossRef] [PubMed]

20. Lee, R.; Kumaresan, Y.; Yoon, S.Y.; Um, S.H.; Kwon, I.K.; Jung, G.Y. Design of gold nanoparticles-decorated $SiO_2@TiO_2$ core/shell nanostructures for visible light-activated photocatalysis. *RSC Adv.* **2017**, *7*, 7469–7475. [CrossRef]

21. Cai, X.G.; He, J.Y.; Chen, L.; Chen, K.; Li, Y.L.; Zhang, K.S.; Jin, Z.; Liu, J.Y.; Wang, C.M.; Wang, X.G.; et al. A 2D-g-C_3N_4 nanosheet as an eco-friendly adsorbent for various environmental pollutants in water. *Chemosphere* **2017**, *171*, 192–201. [CrossRef] [PubMed]

22. Ma, Y.M.; Liu, H.L.; Han, Z.Z.; Yang, L.B.; Liu, J.H. Non-ultraviolet photocatalytic kinetics of $NaYF_4$:Yb,Tm@TiO_2/Ag core@comby shell nanostructures. *J. Mater. Chem. A* **2015**, *3*, 14642–14650. [CrossRef]

23. Yang, J.K.; Lee, S.M. Removal of Cr(Vi) and humic acid by using TiO_2 photocatalysis. *Chemosphere* **2006**, *63*, 1677–1684. [CrossRef] [PubMed]

24. Huang, X.H.; Leal, M.; Li, Q.L. Degradation of natural organic matter by TiO_2 photocatalytic oxidation and its effect on fouling of low-pressure membranes. *Water Res.* **2008**, *42*, 1142–1150. [CrossRef] [PubMed]

25. Zhu, B.S.; Jia, Y.; Jin, Z.; Sun, B.; Luo, T.; Yu, X.Y.; Kong, L.T.; Huang, X.J.; Liu, J.H. Controlled synthesis of natroalunite microtubes and spheres with excellent fluoride removal performance. *Chem. Eng. J.* **2015**, *271*, 240–251. [CrossRef]

26. Wu, S.B.; Zhang, K.S.; Wang, X.L.; Jia, Y.; Sun, B.; Luo, T.; Meng, F.L.; Jin, Z.; Lin, D.Y.; Shen, W.; et al. Enhanced adsorption of cadmium ions by 3D sulfonated reduced graphene oxide. *Chem. Eng. J.* **2015**, *262*, 1292–1302. [CrossRef]

27. Wang, X.D.; Caruso, R.A. Enhancing photocatalytic activity of titania materials by using porous structures and the addition of gold nanoparticles. *J. Mater. Chem.* **2011**, *21*, 20–28. [CrossRef]

28. Mills, A.; LeHunte, S. An overview of semiconductor photocatalysis. *J. Photochem. Photobiol. A* **1997**, *108*, 1–35. [CrossRef]

29.　Yang, J.; Dai, J.; Chen, C.C.; Zhao, J.C. Effects of hydroxyl radicals and oxygen species on the 4-chlorophenol degradation by photoelectrocatalytic reactions with TiO_2-film electrodes. *J. Photochem. Photobiol. A* **2009**, *208*, 66–77. [CrossRef]

30.　Li, X.H.; Chen, G.Y.; Yang, L.B.; Jin, Z.; Liu, J.H. Multifunctional Au-coated TiO_2 nanotube arrays as recyclable SERS substrates for multifold organic pollutants detection. *Adv. Funct. Mater.* **2010**, *20*, 2815–2824. [CrossRef]

31.　Muggli, D.S.; McCue, J.T.; Falconer, J.L. Mechanism of the photocatalytic oxidation of ethanol on TiO_2. *J. Catal.* **1998**, *173*, 470–483. [CrossRef]

32.　Tang, Y.N.; Di, W.H.; Zhai, X.S.; Yang, R.Y.; Qin, W.P. NIR-responsive photocatalytic activity and mechanism of $NaYF_4$:Yb,Tm@TiO_2 core-shell nanoparticles. *ACS Catal.* **2013**, *3*, 405–412. [CrossRef]

33.　Zhang, Y.X.; Yu, X.Y.; Jia, Y.; Jin, Z.; Liu, J.H.; Huang, X.J. A facile approach for the synthesis of Ag-coated Fe_3O_4@TiO_2 core/shell microspheres as highly efficient and recyclable photocatalysts. *Eur. J. Inorg. Chem.* **2011**, *2011*, 5096–5104. [CrossRef]